Chapter 7
Modeling of Process Machine Interactions in Tool Grinding

M. Deichmueller, B. Denkena, K. M. de Payrebrune,
M. Kröger, S. Wiedemann, A. Schröder, and C. Carstensen

Abstract. A systematic modeling approach to predict and manipulate the static and dynamic process machine interactions in tool grinding is described. The modeling approach is verified by experimental investigations gained by means of an industrial tool grinding machine and separate test stands. It combines models of the static and dynamic behavior of the grinding machine and its components with a microscopic grinding process model. Material removal algorithms are applied to cope with the changing shape and changing mechanical properties of the workpiece during grinding. The interaction model has been applied in the process planning phase to optimize tool paths and process parameters in order to reduce resulting shape errors in ground tools.

7.1 Introduction

High performance cutting tools play an important role in modern manufacturing. Within the production of an aircraft, for example, high-quality parts have to be manufactured containing up to several thousand holes with low tolerances. Parts produced for the car industry are also mostly high quality parts. In order to meet the high quality requirements, even for high lot sizes, cutting tools made of tungsten carbide are used, which is a very hard and strong material. In addition, a high effort is spent on machine tests within the process ramp-up phase with the intention of ensuring a fast and stable process. The worldwide market for cutting tools has a volume of about 13 billion € [1], which also shows the significance of the industry.

Due to the hardness of tungsten carbide cutting tools are manufactured by grinding processes. As summarized in part I of this book, many research projects have focused on understanding and controlling grinding processes [2]. In recent years, the focus of research was widened to investigate the influence of the grinding machine to the grinding process, i.e. the process machine interaction. In the grinding of cylindrical cutting tools like drills or end-mills, the workpiece plays an important role regarding the process machine interactions. The relatively low stiffness of the workpiece – which also changes considerably during grinding – leads to static deflections and vibrations and therefore to geometry errors on the ground tool. In order to understand and predict the process machine interaction in

B. Denkena and F. Hollmann (Eds.): Process Machine Interactions, LNPE, pp. 143–176.
springerlink.com

tool grinding it is essential to model both the generation of forces and the generation of deflections.

In the future, the process machine interaction should be considered in the planning phase of tool grinding processes to allow the fabrication of high quality tools with low tolerances and without extensive prototype grinding. Within an interdisciplinary research project of production engineers, mechanical engineers and mathematicians, the authors developed a multi-scale simulation approach, which represents the process-machine interactions in tool grinding in the microscopic and the macroscopic scale.

Tungsten carbide tools are produced using deep grinding processes. Within one production step, the flutes are ground, which can be up to several millimeters deep, see Figure 7.1.

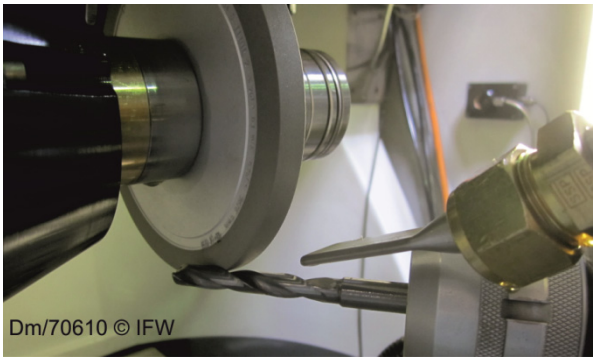

Fig. 7.1 Experimental setup for tool grinding

The occurring process forces lead to large deformations of the workpiece. Therefore, it is modeled by an elastic beam model with changing moments of inertia. In addition, the mechanical properties and dynamic transfer behavior of workpiece clamping, grinding wheel-spindle-system and machine structure are considered in the boundary conditions. Another significant issue is the exact modeling of the occurring grinding forces. The stress distribution and, with this, the grinding forces are dependent on the present process parameters, such as grinding velocity, infeed and the shape of the contact area between grinding wheel and workpiece. The challenge in predicting the grinding forces in tool grinding is that process parameters, such as contact length or depth of cut, are not constant within the contact area and change during grinding.

7.2 Modeling Approach

The modeling approach, which is presented in this paper, has been developed in an interdisciplinary collaboration of the Institute of Production Engineering and Machines Tools (IFW, Leibniz Universität Hannover), the Institute for Machine Elements, Design and Manufacturing (IMKF, TU Bergakademie Freiberg) and the

Department of Mathematics (IfM, Humboldt-Universität zu Berlin). It combines a kinematic-based discrete material removal simulation with a detailed analysis of the current contact area. With this, the current macroscopic shape of workpiece and contact area can be computed considering local contact lengths and cutting depths. Based on the contact analysis, a 3D finite element model for single and multi-grain scratches is parameterized, which allows the calculation of the stress distribution during the microscopic grain engagements. The microscopic grinding force model is also the basis for the dynamic interaction model, which has been developed to predict instable grinding conditions and consider the effect of machine and workpiece vibrations on the resulting grinding process. The modeling approach is consequently validated by experimental data gained by means of an industrial tool grinding machine and with tool grinding tests. The interrelation of the macroscopically and microscopically-based models is illustrated in Figure 7.2.

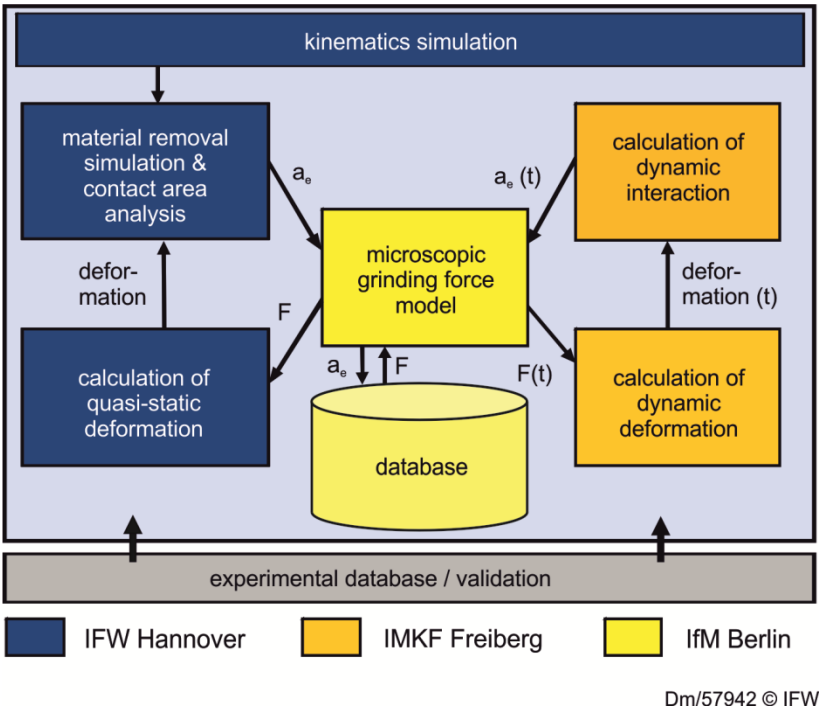

Fig. 7.2 Modeling concept for the simulation of the process machine interactions in tool grinding, interfaces and responsible research institutes

7.3 Modeling of the Machine Structure

Tool grinding machines are flexible machines with a high degree of freedom and normally five machine axes. For experimental analysis of the process machine interactions in tool grinding, a Walter Helitronic Power 5-axis tool grinding machine

is used. Via two axes, the spindle and grinding wheel can be positioned axially in *y* and *z*-direction, whereas the position of the machine table can be defined over one axial (*x*-direction) and two rotation axes (A and C), as illustrated in Figure 7.3.

During the grinding process, forces occur, which deform the machine structure. Since this has an effect on the quality of the produced workpiece, analyses were carried out to characterize the deformation of the clamping of workpiece and grinding wheel and the machine structure.

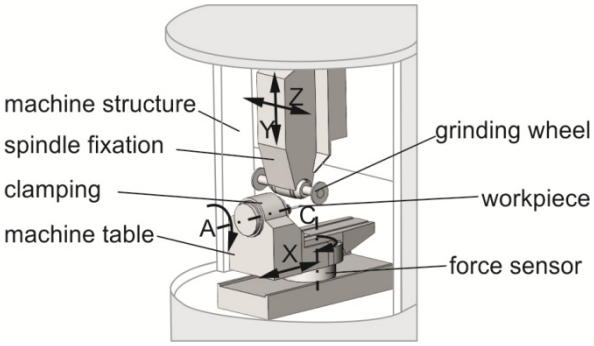

Fig. 7.3 Axis configuration of the used 5-axis CNC tool grinding machine (Walter Helitronic Power)

7.3.1 Workpiece Clamping

The workpiece is fixed on the machine table via a jaw chuck. During the manufacturing process, the workpiece rotates around its center line and moves towards the grinding wheel to realize a helical flute. Thereby, the out-of-roundness and the deformation of the clamping have an impact on the final geometry. Both effects can be measured by tactile sensors during grinding tests. Therefore, an additional measuring pin is added on the workpiece rod.

At the beginning of the grinding tests, the workpiece rotates 5 times before the grinding wheel gets in contact. During grinding, the deformations in *y* and *z*-direction of the workpiece are measured at the cylindrical pin at the tip of the workpiece, as shown in Figure 7.4. Additionally, the corresponding process forces in *y*-direction are displayed as well, see also [3].

In the first 30 seconds, the out-of-roundness of about 37 µm is noticeable in this case. Comparing the amplitude of the sine waves with the largest deformation of the workpiece of 315 µm, the deviation in form and position by the out-of-roundness amounts to 12 % and cannot be neglected. In the workpiece model, the out-of-roundness is thereby realized by an eccentric pre-positioning of the workpiece, which 100 mm long with a diameter of 10 mm.

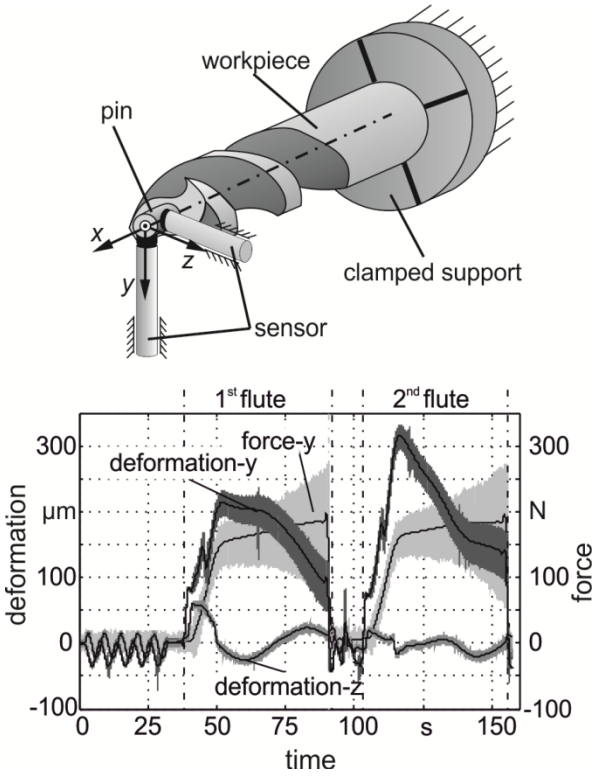

Fig. 7.4. Measurement of workpiece deformation, process forces and out-of-roundness of the workpiece tip

7.3.2 Machine Table

In a separate test, the elasticity of the machine table is analyzed. To measure the deformation of the clamping and the workpiece table a constant force $F = 100$ N is loaded onto the workpiece and the deformation is measured at several positions. The comparison of the measured data and the analytical solution for the static bending of the workpiece rod with ideal stiff boundary conditions results in a linear difference, which can be assigned to the deformation of the machine structure. From Figure 7.5 it can be seen that the calculated difference between measured and calculated deflection curve of a workpiece (10 mm diameter, 100 mm length) amounts to $\Delta y = 11.8$ µm and the tilt to $\Delta\varphi = 1.1\ 10^{-3}$ degrees at the support.

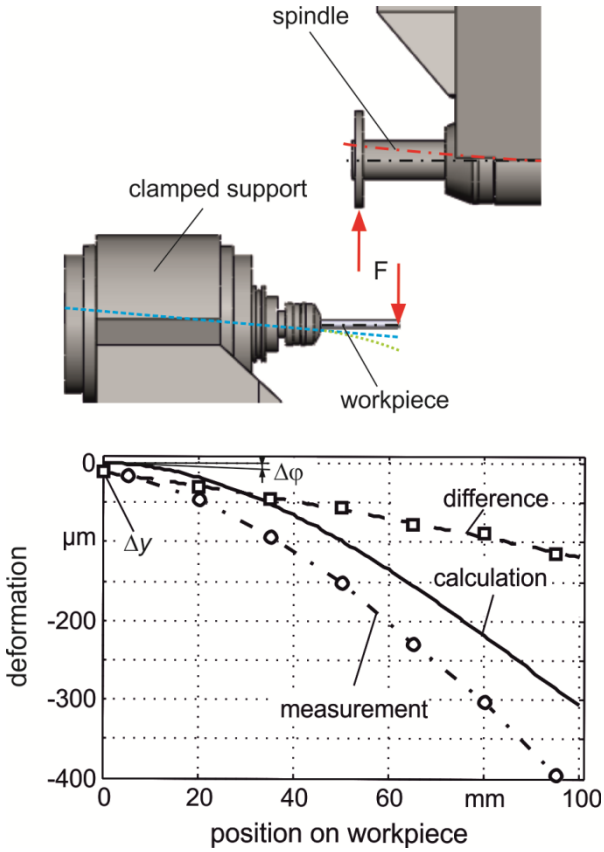

Fig. 7.5 Measured deformation of workpiece and machine table for a constant load of $F = 100$ N

Since the stiffness of the clamping support has an influence on the total displacement of the workpiece, the elasticity of the machine table is implemented into the workpiece model. Therefore, two spring elements are considered in the model with a distance of 40 mm within the clamping, see also [4, 5].

7.3.3 Grinding Wheel Clamping

The elasticity of the spindle is measured in the same way as the deformation of the machine table, see Figure 7.5. A constant force is loaded on the spindle and the deformation is measured at different points. The stiffness of the spindle is detected to $c_{\text{Spindle}} = 11.8$ N/µm, which is in the same range of the stiffness of the clamping and about 30 times higher than the stiffness of the workpiece with an elasticity of about $c_{\text{Workpiece}} = 0.4$ N/µm measured at the tip of the workpiece. The deformation of the spindle influences the contact conditions during the grinding process, therefore the elasticity has to be considered in the model, especially for modeling the dynamic movement of the spindle during grinding.

7.3.4 Grinding Wheel

To manufacture super-hard cutting materials like high speed steels or tungsten carbide, grinding wheels with diamond or CBN-grains are used. The abrasive grains are placed in a bonding, where additives are implemented to improve the heat conductivity or to enlarge the chip space for better chip removal and coolant supply. Before grinding, the grinding wheel has to be trued and sharpened. With the truing process, the macroscopic shape of the grinding wheel is defined. During sharpening, the bond is set back until sharp grains appear on the surface of the grinding wheel and sufficient chip space is created. This conditioning process is necessary because the grinding wheel wears over time meaning that the abrasive grains blunts or break out and the shape of the wheel changes.

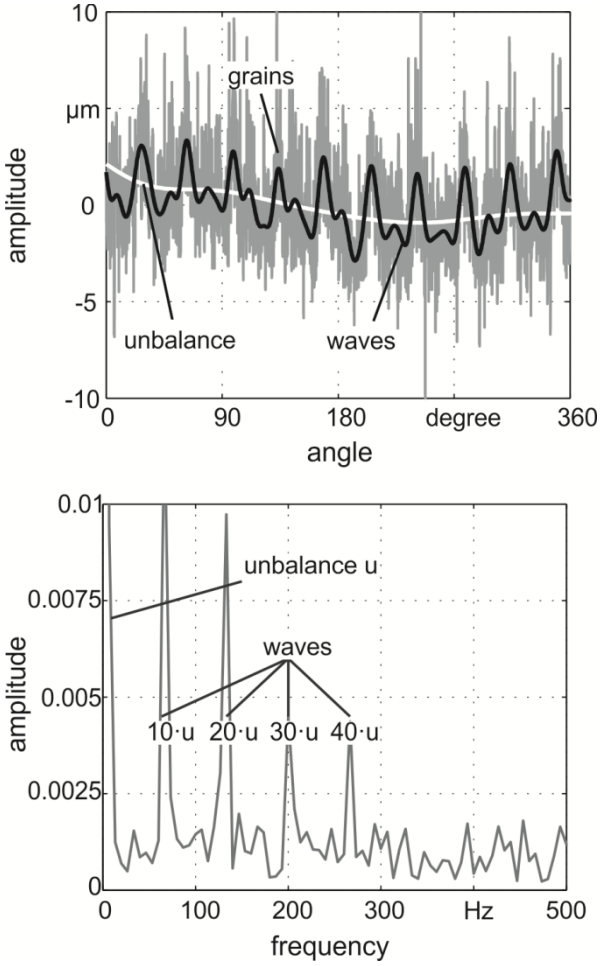

Fig. 7.6 Measured surface and Fast Fourier analysis of a grinding wheel topography with graining D91

The contact between grinding wheel and workpiece is characterized by thousands of stochastically microscopic grain engagements. These grain contacts dynamically excite the system, which can cause chatter or lifting and has a negative effect on the quality of the ground surface. The corrugation of the grinding wheel surface and the excitation frequency are mainly dependent on the rotation speed $2\pi n$. Therefore, the shape of a nominally cylindrical grinding wheel is measured by a laser sensor and analyzed. The measured data are shown in Figure 7.6. It is obvious that the grinding wheel surface is wavy with different frequencies, as shown by the Fourier transformation. The fundamental oscillation is due to an out-of-roundness of the wheel with the basic frequency n of the rotation speed whereas the harmonics are based on additional waves. The high-frequency noise corresponds to the abrasive grains. Since the size of the grains, which overlap over the bonding, is nearly normally distributed, as references and analysis have shown, it can be described mathematically, [6]. To represent the high-frequency excitation of the workpiece in the dynamic simulation the grinding wheel is modeled by a combination of sine waves for the out-of-roundness and the periodic waves, and additionally by a normal distribution for the grains. The amplitudes are taken from measurements, see also [3].

7.3.5 Workpiece Model

The workpiece is considered to be one part of the whole structure which interacts with the tool grinding process. The modeling approach for the workpiece consists of two parts. The first part is responsible for modeling the current macroscopic shape of the workpiece. The workpiece geometry and material removal are discretized using a so-called dexel model. The second part describes the static and dynamic deflection of the workpiece deformation. Here, the Euler beam equation and a finite element approach with beam elements, respectively, are applied. Both parts of the workpiece model are described in detail below.

7.3.5.1 Dexel Model

In 1986, van Hook introduced “dexels” or “depth elements” as a discretization method for workpieces [7]. Since then, dexels have been applied by several authors for the simulation of manufacturing processes, e. g. [8, 9]. The workpiece is discretized by a regular grid of dexels, which have a constant distance in two directions and varying lengths in the third direction. The accuracy of the model is high in dexel direction and relatively low perpendicular to it. The use of three independent dexel grids overcomes the problem of different model accuracy in the coordinate directions. Figure 7.7 shows the discretization of the workpiece with dexel grids in all three coordinate directions. A dexel $D_{i,j}$ can be identified by the position i,j in the particular dexel grid. Undercuts can be simulated by adding a dexel segment $D_{i,j,d}$ to the current dexel.

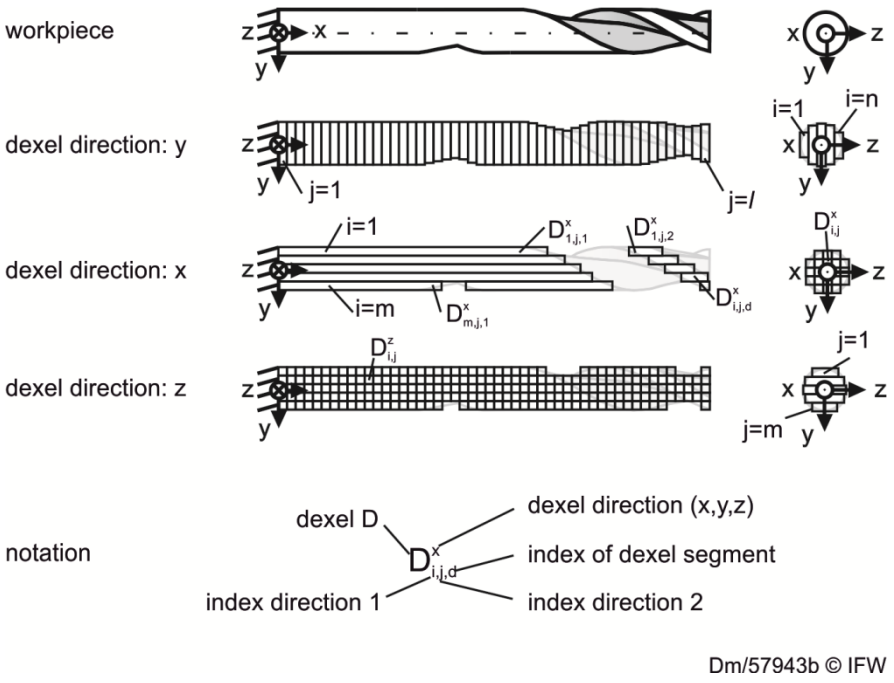

Fig. 7.7 Workpiece discretization with dexels

The cylindrical grinding wheel is approximated as a non-rotating polyhedron in the easiest case. The movement of the grinding wheel is determined by a NC-program, which can be interpreted by the simulation system. During one simulation step, the grinding wheel moves from one position to the next in a stepwise linear movement. The trace of the grinding wheel is called the sweep volume. In each simulation step, the intersection of sweep volume and workpiece is calculated. In case of an intersection, the specific dexels are shortened, divided or removed [10].

7.3.5.2 Static Deformation

In each simulation step, the current workpiece's cross sections are analyzed for calculating the geometrical moments of inertia I_{yy}, I_{zz} and I_{yz} at discrete positions x_i along the workpiece axis x. For example, the geometrical moment of inertia I_{zz} can be calculated with

$$I_{zzD} = \frac{b_D \cdot h_D^3}{12} + y_D^2 \cdot b_D \cdot h_D, \qquad I_{zz} = \Sigma I_{zzD} \tag{1}$$

as displayed in Figure 7.8.

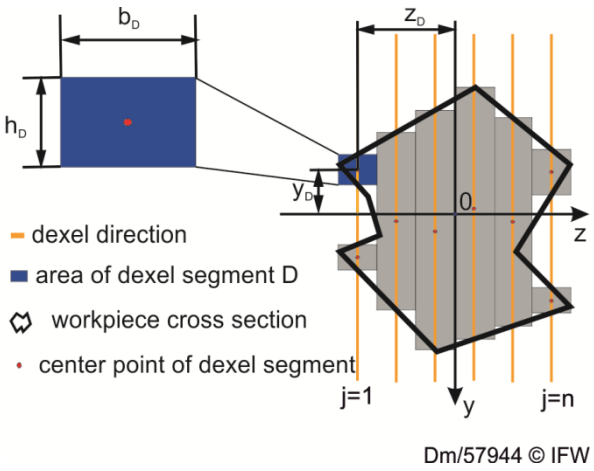

Fig.7.8 Calculation of geometrical moments of inertia

The static oblique bending of the workpiece is calculated by integrating the linear beam equations

$$v''(x) = \frac{-I_{yz}(x)M_y(x) + I_{yy}M_z(x)}{E(I_{yy}I_{zz} - I_{yz}^2)},$$
$$w''(x) = \frac{-I_{zz}(x)M_y(x) + I_{yz}M_z(x)}{E(I_{yy}I_{zz} - I_{yz}^2)} \quad (2)$$

in every simulation step, where v is the deformation in y-direction and w in z-direction. The material (tungsten carbide) is assumed to be isotropic and homogeneous, with Young's modulus E being 590,000 N/mm². In addition to the geometrical moments of inertia $I(x)$, the bending moments M are a function of position x and time t. To determine $M(x)$ a grinding force model is applied, which is described in Section 7.4.2. In case the clamping is assumed to be rigid, the boundary conditions are $v(0) = w(0) = 0$ and $v'(0) = w'(0) = 0$ or otherwise dependent on the stiffness of the support. After calculating the bending lines $v(x)$ and $w(x)$ the deformation at position x_i is assigned to all dexels of dexel layer i.

7.3.5.3 Dynamic Deformation

The dynamic workpiece deflection is highly dependent on the momentary geometry, stiffness and forces loaded on the workpiece. Mathematical and experimental investigations have shown the dependencies of the eigenfrequencies on the length

ℓ of the ground flute and depth of cut a_e. In Figure 7.9, the first eigenfrequency of a workpiece with longitudinal flutes is shown exemplarily. The variation of the workpiece characteristics is visible. A finite beam element approach is used as workpiece discretization, according to the dexel model, to represent the changing properties, compare [11].

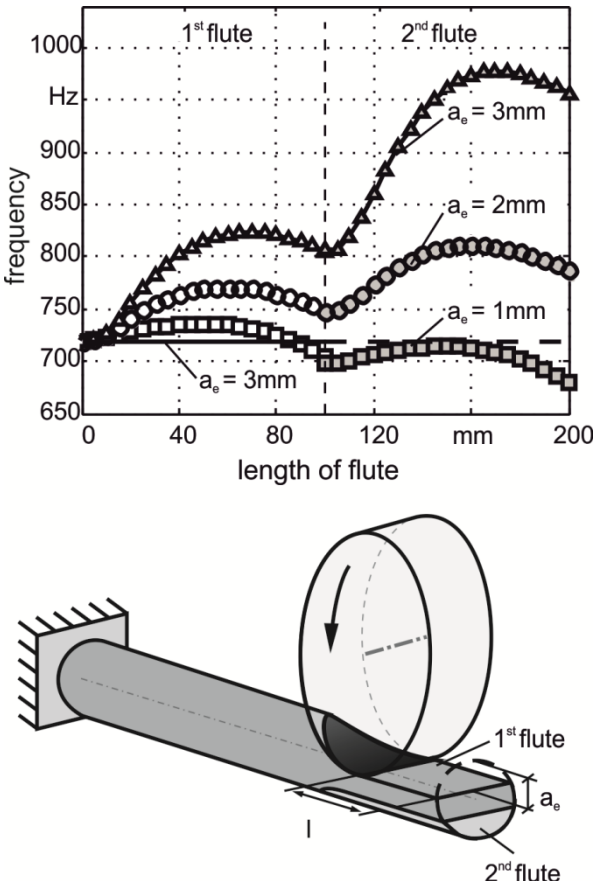

Fig.7.9 Simulated workpiece frequency characteristics depending on the geometry for longitudinal ground flutes

Each beam element has six degrees of freedom to represent bending and torsion of the workpiece axis. The properties are assumed to be constant within one element but can change over time. The equation of motion can be written as

$$\mathbf{M}\ddot{\mathbf{q}} + \mathbf{D}\dot{\mathbf{q}} + \mathbf{K}\mathbf{q} = \mathbf{f}, \tag{3}$$

with the mass matrix **M,** the damping matrix **D**, the stiffness matrix **K**, the vector of the generalized coordinates **q** and the vector of forces and moments **f**. Because the system of coupled equations has the size of $6n \times 6n$, with n the number of elements, it is very large and takes long to solve. By means of a modal reduction, the system can be reduced and the equations become linearly independent, which simplifies the solving process. The modal transformation of the system in the modal space is carried out by a transformation matrix $\mathbf{\Phi} = \left[\hat{\mathbf{q}}_\mathbf{1}, \hat{\mathbf{q}}_\mathbf{2}, ..., \hat{\mathbf{q}}_\mathbf{n}\right]$ with $\hat{\mathbf{q}}_\mathbf{i}$ the eigenvectors of the system. Via the substitution of the node displacements

$$\mathbf{q} = \mathbf{\Phi} \mathbf{q}_{\mathbf{mod}} \tag{4}$$

and the multiplication with the transformation matrix from the left side the equation of motion can be written in modal space as

$$\begin{aligned} &\mathbf{\Phi}^{\mathrm{T}} \mathbf{M} \mathbf{\Phi} \ddot{\mathbf{q}}_{\mathrm{mod}} + \mathbf{\Phi}^{\mathrm{T}} \mathbf{D} \mathbf{\Phi} \dot{\mathbf{q}}_{\mathrm{mod}} + \mathbf{\Phi}^{\mathrm{T}} \mathbf{K} \mathbf{\Phi} \mathbf{q}_{\mathrm{mod}} = \mathbf{\Phi}^{\mathrm{T}} \mathbf{f} \\ &\mathcal{M} \ddot{\mathbf{q}}_{\mathrm{mod}} + \mathcal{D} \dot{\mathbf{q}}_{\mathrm{mod}} + \mathcal{K} \mathbf{q}_{\mathrm{mod}} = \mathbf{f}_{\mathrm{mod}} \end{aligned} \tag{5}$$

By using special eigenvectors the modal mass matrix $\mathcal{M}$ is equal to the identity matrix; and the modal stiffness matrix has a diagonal shape $\mathcal{K} = diag\{\omega_1^2, \omega_2^2, ..., \omega_n^2\}$ with the eigenvalues as entries. Depending on the number of considered eigenvectors, the size of the system is reduced in modal space; however the information about the neglected modes is also lost.

The reduction of Equation (5) to a system of first order with the substitution $\mathbf{z}_1 = \mathbf{q}_{\mathrm{mod}}$ and $\mathbf{z}_2 = \dot{\mathbf{q}}_{\mathrm{mod}}$ is

$$\begin{aligned} \frac{d}{dt}\begin{bmatrix} \mathbf{z}_1 \\ \mathbf{z}_2 \end{bmatrix} &= \begin{bmatrix} \mathbf{0} & \mathbf{E} \\ -\mathcal{M}^{-1}\,\mathcal{C} & -\mathcal{M}^{-1}\,\mathcal{D} \end{bmatrix} \begin{bmatrix} \mathbf{z}_1 \\ \mathbf{z}_2 \end{bmatrix} + \begin{bmatrix} \mathbf{0} \\ \mathcal{M}^{-1}\mathbf{f}_{mod} \end{bmatrix}, \\ \dot{\mathbf{z}} &= \mathcal{A}\,\mathbf{z} + \mathbf{f}(t). \end{aligned} \tag{6}$$

The solution of the dynamic deformation of the excited system is a combination of a homogeneous and a particular solution. To apply the method of variation of constants to Equation (6) a general solution is given by

$$\mathbf{z}(t) = e^{\mathcal{A}t}\,\mathbf{z}(t_0) + \int_0^t e^{\mathcal{A}(t-\tau)}\,\mathbf{f}(\tau)\,d\tau \ . \tag{7}$$

To calculate the momentarily dynamic deformation the solution is determined step-wise. This means that the solution for time $\mathbf{z}(t_i+\Delta t)$ is determined depending on the last solved step $\mathbf{z}(t_i)$, the step size Δt and the momentary excitation of $\mathbf{f}(t_i)$. It is assumed that the momentary excitation $\mathbf{f}(t_i)$ is constant within the small step

size Δt. The matrix $\mathcal{A}$ depends on the geometry of the workpiece and has been recalculated frequently.

After solving Equation (7) in modal space, the solution of the deformation has to be retransformed into the physical space by Equation (4).

7.4 Tool Grinding Process Model

In addition to the detailed mathematical description of the relevant parts of the machine structure in Section 7.2, a model describing the tool grinding process itself is needed to predict the process machine interaction. Tool grinding is characterized by contact conditions between grinding wheel and workpiece, which are more complex than in conventional surface grinding. During the grinding of the helical flutes, the workpiece is fed into the grinding wheel with a helical movement. The shape of the grinding wheel in combination with the relative movement of workpiece and grinding wheel generates the shape of the flute. The contact area has a complex shape with a variation of contact lengths and cutting depths. The basis for the grinding force modeling is a detailed geometrical analysis of the contact area, which is described in the following.

7.4.1 Model-Based Contact Area Analysis

To build a grinding process model, which can calculate the three dimensional distribution of the grinding stresses and the resulting load in tool grinding, a geometrical analysis of the contact area is necessary. The analysis is based on the dexel model described in 7.3.5.1, where each dexel represents one fraction of the total workpiece volume. In each simulation step, dexels intersecting with the grinding wheel are shortened or removed. A big change in dexel length represents a high material removal rate and vice versa. By dividing the removed volume V_D of each dexel i by the simulation time step size Δt, the distribution of the material removal rate Q_{wa} in the contact area can be determined.

$$Q_{wa}(i) = V_D(i) / \Delta t. \tag{8}$$

Figure 7.10 a) exemplarily shows the occurring external material removal rates Q_{wa} for a flute grinding process.

As described in [12], the external material removal rate $Q_{wa}(i)$ is used to determine the equivalent chip thickness h_{eq} for each volume element, see Figure 7.10 b). For the calculation, a constant cutting speed v_c is assumed, which is reasonable due to the cylindrical shape of the grinding wheel. With the presented procedure, it is possible to determine equivalent grinding parameters like h_{eq} and Q_{wa} for every dexel cut during one simulation step. It can be applied for changing contact geometries and an arbitrary grinding wheel movement. The contact area analysis is the basis for the application of grinding force models, which are described in the following section.

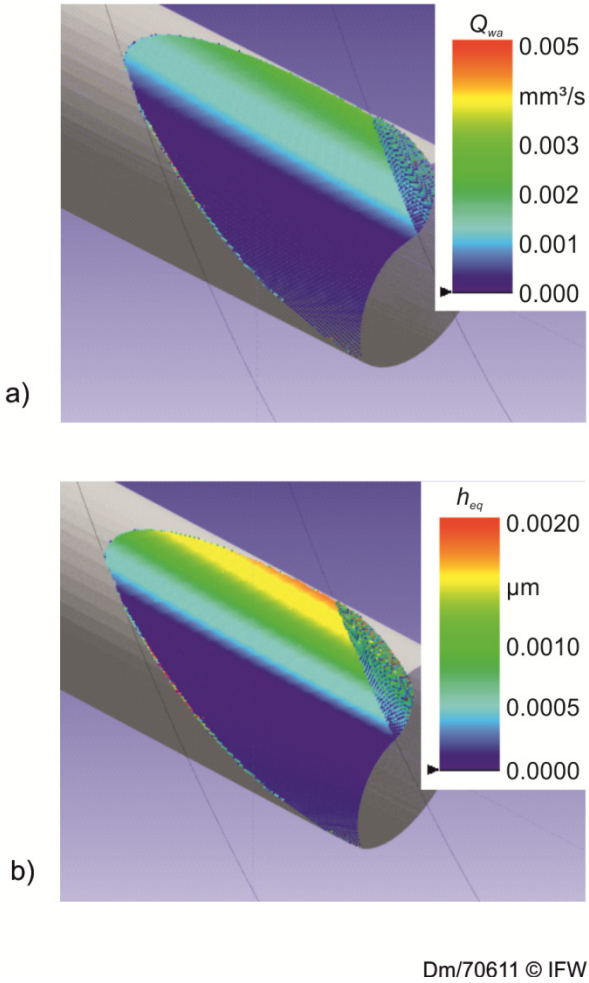

Fig. 7.10 a) Calculated material removal rate Q_{wa}(i) [mm³/s] and b) calculated equivalent chip thickness h_{eq} [µm] for a tool grinding process (v_{ft} = 30 mm/min, d = 10 mm, R = 62.0 mm)

7.4.2 Grinding Force Model

Two approaches for calculating the grinding forces are shown. Both use the equivalent grinding parameters as input data. The microscopic finite element approach calculates the stress resulting from a single grain – workpiece contact. The second approach determines the grinding force distribution empirically.

7.4.2.1 Microscopic Force Model

Within the tool grinding process, the interaction of grains and workpiece on a microscopic scale result in forces observable on a macroscopic scale. These forces

are measured under the machine table, see Figure 7.3, but experiments suggest that the stresses vary throughout the contact zone. In order to include this variation, a process force model has to account the locally different contact conditions. The contact zone is discretized into small sub-domains by the dexel model (see 7.2.5.1). The range of parameters for the engagement of single grains can be calculated using the geometrical analysis explained in 7.3.1. and [12]. This analysis also provides a method for the combination of the microscopic stresses stored in a database (see Figure 7.2) to the stress distribution within the contact zone. Here, the approach is to model the contact of grains and workpiece on a microscopic scale for the different parameters of those sub-domains. This is carried out by coupling variational inequalities describing the elasto-plastic behavior of the workpiece and its contact with abrasive grains. Linear kinematic hardening is assumed for the workpiece on microscopic scale denoted by $\mathbf{\Omega}$. This domain is fixed on the free boundary $\mathbf{\Gamma}_D$; and the contact boundary is denoted by $\mathbf{\Gamma}_C$. For the case of notation, only one time-step of the quasi-static problem with initial values set to zero is considered here (for further details see [13]). The primal problem of elasto-plasticity with linear kinematic hardening including contact is to find a displacement field $\mathbf{u}$ and a plastic strain $\mathbf{P}$ such that

$$\begin{aligned} -\operatorname{div}\sigma(\mathbf{u},\mathbf{P}) &= f \text{ in } \Omega, \\ \sigma(\mathbf{u},\mathbf{P}) &= \mathbb{C}\varepsilon(\mathbf{u}) - \mathbf{P}, \\ \mathbf{u} &= 0 \text{ on } \Gamma_D, \\ \sigma_n(\mathbf{u},\mathbf{P}) &= t_0 \text{ on } \Gamma_N, \\ \mathbf{u}_n \le g;\ \sigma_n \le 0;\ (\mathbf{u}-g)\sigma_n &= 0 \text{ on } \Gamma_C, \\ \sigma(\mathbf{u},\mathbf{P}) - \mathbb{H}\mathbf{P} &\in \partial j(\mathbf{P}). \end{aligned} \tag{9}$$

Here, $j(\mathbf{Q}) := \int_\Omega \sigma_y (\mathbf{Q}:\mathbf{Q})^{1/2}$, is the non-differentiable part of the minimum plastic work function with the yield stress $\sigma_y > 0$ in uni-axial tension, σ denotes the stress, $\mathbb{C}$ is the elasticity tensor and $\mathbb{H}$ is the tensor describing the hardening. For simplicity, the surface traction t_0 and the outer volume force f are assumed to be zero from here on. $\mathbf{M} : \mathbf{N} := M_{ij}N_{ij}$ denotes the usual scalar product of $\mathbf{M}$ and $\mathbf{N}$. The part of the boundary $\mathbf{\Gamma}_N$ is assumed to be disjoint with $\mathbf{\Gamma}_D$ and $\mathbf{\Gamma}_C$.

Since the unique analytic solution $\mathbf{W} := (\mathbf{u}, \mathbf{P})$ for this partial differential equation and inclusion is generally unknown, a numerical approximation has to be computed. For this purpose, the mathematical problem shown in (9) is reformulated as a variational inequality; and then it is equivalently written as a saddle-point problem introducing Lagrange multipliers. Moreover, the spaces, where the solution is searched, are replaced by discrete ones. This results in the problem to find $\mathbf{W}_h$, $\lambda_{C,H}$, $\lambda_{p,h}$ such that

$$\begin{aligned} a(\mathbf{W}_h, \mathbf{Z}_h) + \int_{\Gamma_C} \lambda_{C,H}\mathbf{v}_h \cdot \mathbf{n} + \int_\Omega \sigma_y \lambda_{h,p} : \mathbf{Q}_h = 0 \\ \int_{\Gamma_C} (\mu_{C,H} - \lambda_{C,H})\mathbf{u}_h \cdot \mathbf{n} + \int_\Omega \sigma_y (\mu_{p,h} - \lambda_{p,h}) : \mathbf{Q}_h \le 0 \end{aligned} \tag{10}$$

for all $(\mathbf{Z}_h, \mu_{C,H}, \mu_{p,h}) \in W_h \times \Lambda_{C,H} \times \Lambda_{p,h}$. Here,

$$a(\mathbf{W}, \mathbf{Z}) := \int_\Omega \mathbb{C}(\varepsilon(\mathbf{u}) - \mathbf{P}) : (\varepsilon(\mathbf{v}) - \mathbf{Q}) + \mathbf{P} : \mathbb{H}\mathbf{Q},$$

where **n** is the outer unit normal. It can be shown that the mathematical problem shown in (10) has a unique solution ($\mathbf{W}_h$, $\lambda_{C,H}$, $\lambda_{p,h}$). $\lambda_{C,H}$ is the approximation of the normal stress on the contact boundary, whereas $\lambda_{p,h}$ is the approximation of the plastic stress, cf. [14,15]. The finite dimensional space $\mathbf{W}_h$ is constructed on hexahedral meshes. In order to ensure the uniqueness of $\lambda_{C,H}$, the discretization of $\mathbf{\Gamma}_C$ is carried out with a mesh-size $H > h$, see [16]. An error estimator presented in Chapter 3 and [17] and an adaptive refinement algorithm allowing possible multi-level hanging nodes, cf. [18,19], are used in order to improve the accuracy of the discrete solution for a fixed number of degrees of freedom.

Another numerical approximation approach is the regularization of the variational problem obtained from Problem (9), which results in an energy minimization problem over $K := \{\mathbf{v} \in H_0^1(\Omega)^3 \mid \mathbf{v}(x)\cdot\mathbf{n}(x) \le g(x) \text{ on } \Gamma_C\}$ of the smooth functional

$$\mathcal{F}(\mathbf{Z}) := \frac{1}{2} a(\mathbf{Z}, \mathbf{Z}) + j_\delta(\mathbf{Z}) \tag{11}$$

where $j_\delta(\mathbf{Z}) := \int_\Omega \sigma_y (\mathbf{Q} : \mathbf{Q} + \delta^2)^{1/2}$, and δ the regularization parameter. In order to use the Newton-Raphson method on the whole space V instead of K, the penalty functional

$$\Psi(\mathbf{v}) := \frac{1}{2\varrho} \int_{\Gamma_C} (\mathbf{v}\cdot\mathbf{n} - g)_+^2 \tag{12}$$

is introduced. Here, ρ is the penalty parameter and $(f)_+ := \max(0, f)$ denotes the positive part of a real valued function f. The functional Ψ is added to the energy functional $\mathcal{F}$; and the finite element space W_h is used to compute a discrete approximation of $\mathbf{W}_{\rho,\delta}$. The main drawback of this approach is its dependence on δ and ρ, cf. [20, 21]. The normal component of the microscopic contact forces F_{micro} is computed from the Lagrange multiplier λ_c via

$$F_{\text{micro}} = \int_{\Gamma_C} \lambda_C . \tag{13}$$

If the regularized energy functional and the Newton-Raphson method are used, the stress must be computed from u with Hooke's law and the normal stress is integrated over the contact boundary. Once parameterized, the computed values are stored in the database and missing entries have to be interpolated or newly computed. This parameterization of the microscopic force model is carried out via the measurement of single grain scratches. Figure 7.11 shows the deformation computed by the finite element approach with regularization after a single grain scratch. The maximum infeed was set to 5 µm; and the grain moved on a circle with a diameter of 150 mm. The red color indicates areas where the plowing effect occurs, i.e. material piles up next to the scratch line. However, the resultant cutting depth is lower than the nominal depth of cut due to the elastic deflection of tool and workpiece.

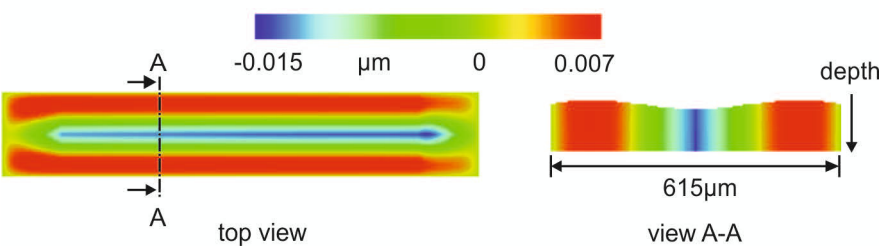

Fig. 7.11 Resulting cutting depth of a simulated scratch test

Here, the results of main interest are the forces occurring during scratching. Figure 7.12 shows the computed forces for different parameter configurations. The change in the module of elasticity has the biggest influence on the forces. This reduction of the module of elasticity could be interpreted as damage to the material. This damage is likely to occur during the scratching itself (for an example of brittle material, see [22]) or could be introduced by the pre-treatment of the workpiece.

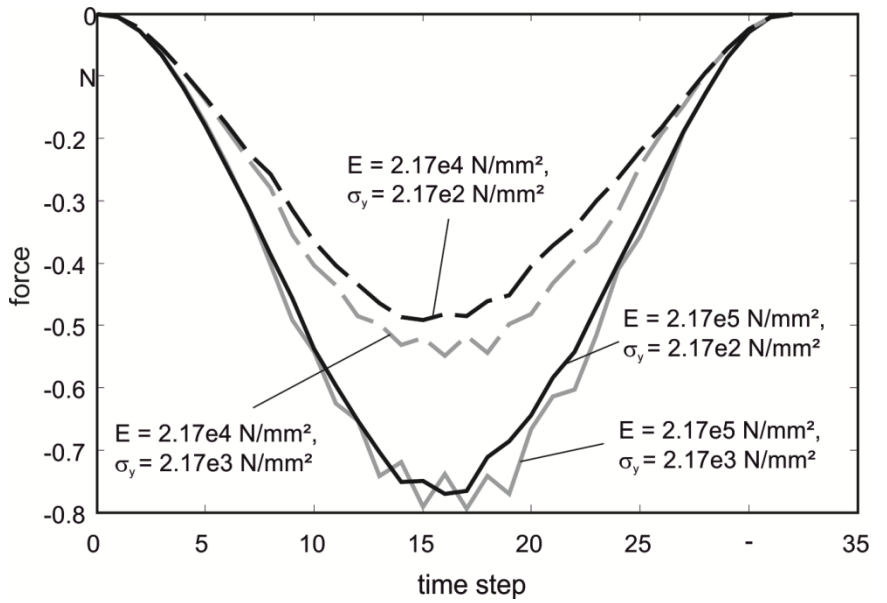

Fig. 7.12 Force during scratch test calculated with microscopic Finite Element simulation

A possible approach to explain macroscopic damage phenomena is based on small cracks on the microscopic level [23]. Both discretizations of the elasto-plastic material law introduced above can be extended to allow fissures. Therefore, the faces between hexahedra in the finite element mesh can be doubled and disconnected. In Figure 7.13, a small crack was introduced based on previously computed stresses. This allows the simulation of crack growth along faces.

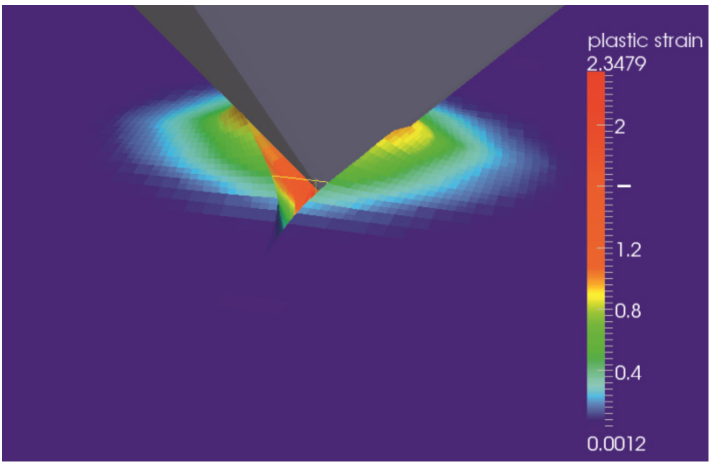

Fig. 7.13 Strain calculation by a Finite Element simulation with a priori crack

7.4.2.2 Empirical Force Model

To parameterize an empirical grinding force model, flat grinding experiments using a cylindrical grinding wheel and a rectangular workpiece have been carried out on a Walter Helitronic Power tool grinding machine. The workpiece has been tightly fixed to the machine table in order to minimize deformation for correct correlation between grinding depth and force, compare Figure 7.14.

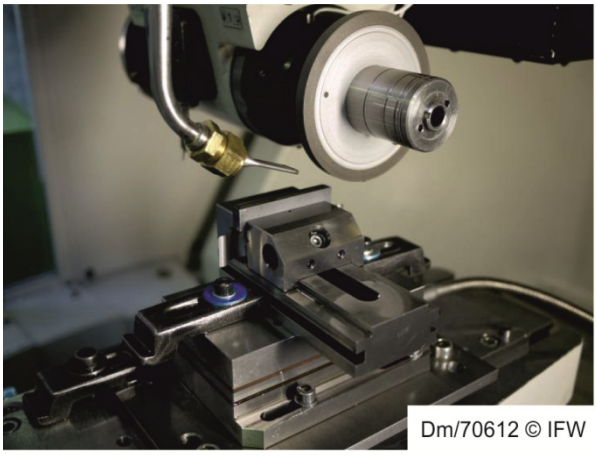

Fig. 7.14 Experimental setup to determine the influence of a_e on grinding forces

A Kistler three-component dynamometer has been used to measure the grinding forces for different depths of cut and feed speeds. As described in [24], the resulting forces for different depths of cut had to be related to geometrical parameters, which can be evaluated both in the experiment, as described above, and in the 3D dexel simulation. The factor h_{eq}/dl_g has been found to suit this requirement well. It relates the equivalent chip thickness h_{eq} to the local contact length dl_g for each segment of the contact area. This dimensionless value replaces the factors feed speed, cutting speed and grinding wheel diameter, which are commonly used in grinding force models [25]. Figure 7.15 shows the relationship between the mechanical stresses and h_{eq}/dl_g.

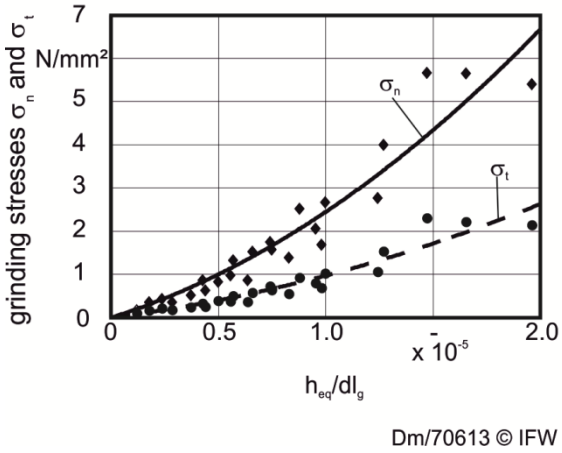

Fig. 7.15 Relationship between mechanical stresses σ_n (solid line, ♦) and σ_t (dashed line,●) and h_{eq}/d_{lg} for a tool grinding process (v_{ft} = 15 - 50 mm/min, a_e = 0.01 - 1mm, v_c = 18 m/s)

The calculated stresses are fitted to a polynomial equation applying the least squares method.

$$\sigma_n = \left(1.56\cdot 10^5 \cdot \frac{h_{eq}}{d_{lg}} + 9.92\cdot 10^9 \cdot \left(\frac{h_{eq}}{d_{lg}}\right)^2\right)\frac{N}{mm^2}$$
$$\sigma_t = \left(0.63\cdot 10^5 \cdot \frac{h_{eq}}{d_{lg}} + 3.43\cdot 10^9 \cdot \left(\frac{h_{eq}}{d_{lg}}\right)^2\right)\frac{N}{mm^2} \quad (14)$$

This relationship is applicable for the parameter range shown in Figure 7.15. The grinding force model has been implemented into the simulation system to visualize the occurring stresses in tool grinding. Figure 7.16 shows the distribution of the normal stresses in the contact area. It can be seen that the highest pressure acts at the area with high equivalent chip thickness h_{eq}, cp. Figure 7.10 b).

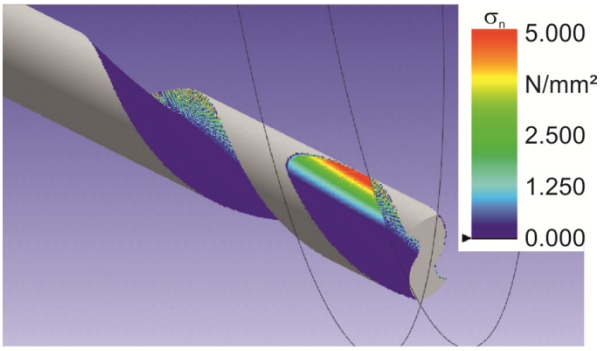

Fig. 7.16 Calculated distribution of normal stress σ_n [N/mm²] for a tool grinding process (v_{ft} = 30 mm/min, d = 10 mm, R = 62.0 mm)

7.4.3 Temperature in Contact Area

A main task in modeling of grinding processes is the determination of the generated heat and its distribution into workpiece, grinding wheel, coolant, chips and environment. Most approaches consider a 2D moving heat source model according to Carslaw and Jaeger with a constant heat flux density throughout the contact area. Applying this heat source model to a workpiece model using linear heat conduction theory and assuming an adiabatic fixturing and an isotropic material model, it is possible to calculate the transient temperature distribution inside the workpiece. However, these approaches are limited to grinding processes with constant engagement along the grinding wheel axis and relatively large workpieces where losses to the environment can be neglected. To determine the heat flux density, one has to know the generated heat and the area of contact. The heat flux into the workpiece is dependent on the temperature acting in the contact area. Therefore, it is a common task in research on grinding processes to determine the temperature in the contact area, which is difficult, since the contact area is not easily accessible by optical temperature measurement equipment like infrared cameras. Also, a high effort is needed to prepare the workpieces when using thermocouples being positioned in different positions inside the workpiece. With this indirect measurement method the temperature in the contact area is calculated by extrapolating the temperatures in different positions inside the workpiece with defined distance to the contact area.

In tool grinding, where the workpieces are relatively small and the ground flutes have a special concave shape it is not feasible to position the thermocouples in a defined position inside the workpiece. The authors chose a measurement setup, where temperature sensor and electronics are inside the grinding wheel, with the advantage that the temperature in the contact area can be measured directly with a measuring range of 150°C – 600°C, see Figure 7.17.

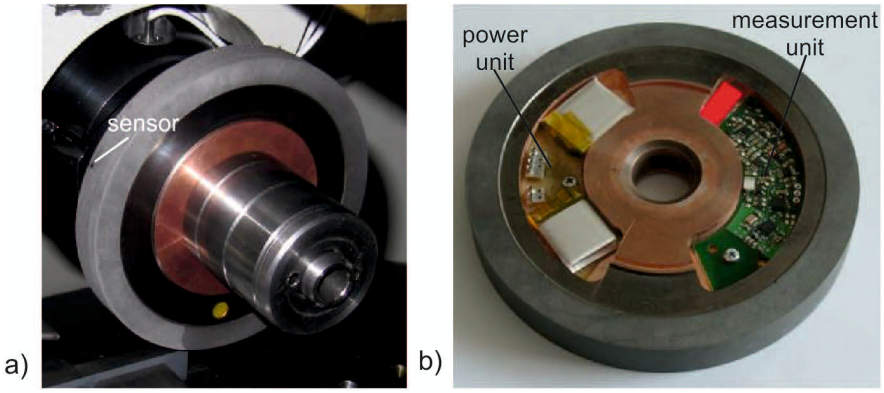

Fig. 7.17 a) Grinding Wheel made by FOS Messtechnik GmbH equipped with a temperature sensor b) electronics inside the grinding wheel with detector, batteries and wireless equipment for sending the data to external receiver during grinding

Figure 7.18 shows measurement results using the sensor integrated grinding wheel. A flute with a helical angle of 30° was ground into a tungsten carbide workpiece with a diameter of 16 mm. It can be seen, that the temperature signal (black line) rises to its maximum level of about 210°C when the grinding wheel is entering the workpiece. The time delay of the temperature signal is due to the fact that the measurement range of the temperature sensor starts at about 150°C. The explanation for the higher signal level at the beginning of the measurement is that the sensor is calibrated for the temperature of tungsten carbide. At the beginning, there is no contact between grinding wheel and the tungsten carbide workpiece and the signal is not valid. The process forces, which are measured in machine tool coordinates (see Figure 7.3), and the measured temperature show similar characteristics: during the constant engagement conditions both, process forces and temperatures stay constant. This characteristic implies that the process is thermo-mechanically stable with constant heat flows due to the flood supply of coolant.

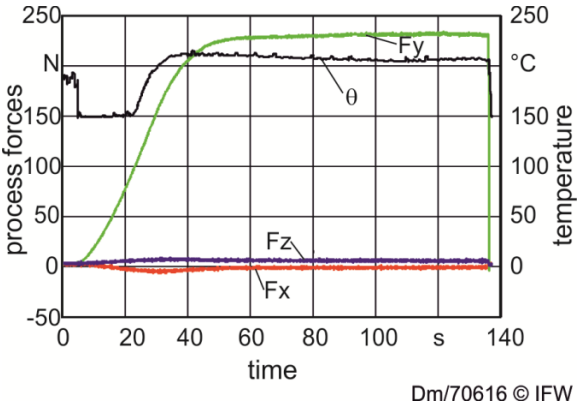

Fig. 7.18 Process forces and temperatures measured with the sensor integrated grinding wheel (v_f = 25 mm/min, v_c = 18 m/s, workpiece diameter d = 16 mm)

With the help of the sensor integrated grinding wheel it is possible to analyze the influence of the coolant supply on the grinding process. Figure 7.19 shows the variation of the coolant jet velocity and the resulting temperature in the contact and the ratio μ between tangential force F_t and normal force F_n. It can be seen, that the lowest temperature and friction occurs when the coolant jet velocity is equal to the cutting speed v_c.

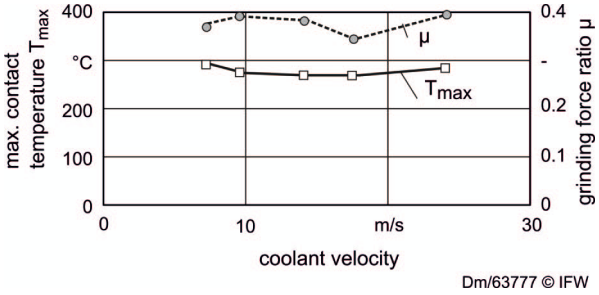

Fig. 7.19 Influence of velocity of coolant on temperature and grinding force ratio (process: v_{ft} = 30 mm/min, v_c = 18 m/s, workpiece diameter: 16 mm, helix angle: 30°, coolant: mineral oil)

7.5 Planning and Optimization of Tool Paths

With the presented models of machine structure, workpiece and tool grinding process it is possible to calculate forces based on a material removal simulation and a contact area analysis. For a prediction of the deflections occurring in tool grinding it is necessary to couple both process model and structure model. Since a deflection directly affects the contact conditions and therefore the acting grinding forces, a coupling of process and structure model using an iterative algorithm is required. The algorithm determines the deformation of workpiece and machine structure during grinding at a static equilibrium of the grinding force and the spring-back force of the workpiece until the residuum between the deformations calculated in the last step and in the current step is smaller than a predefined value ε. Then the material is removed, the actual geometry is defined and the following calculation step is carried out.

Using the prescribed simulation method, a method has been developed to adapt existing tool paths for reducing the effects of process machine interactions in tool grinding. The procedure is described in Figure 7.20. Based on a simulation of the grinding process using the original tool path, the workpiece deflection is calculated. The workpiece deflection is then added to the tool path which means that the grinding wheel cuts more material than before. The simulation and optimization is repeated until the calculated workpiece cross sections are equal to the ideal cross section which is determined by a simulation run with an ideally stiff workpiece.

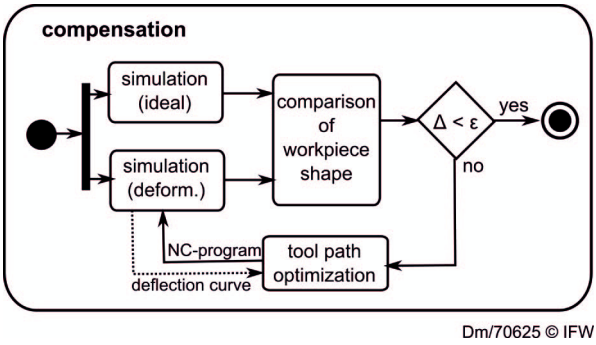

Fig. 7.20 Method for optimizing tool paths in tool grinding

7.6 Application and Results

7.6.1 Simulation of Static Effects

The empirical grinding force model (compare Section 7.4.2.2) has been coupled with the elastic workpiece model described in Section 7.3.5.2 to predict the grinding forces in tool grinding considering the deflection of the workpiece. Figure 7.21 shows a comparison of simulated and measured grinding forces for the parameters listed in the caption. The following effects are visible in the Figure: 1) The mean value of the measured grinding forces matches the simulated forces very well for the first flute, 2) The phases, where the grinding wheel enters and exits the

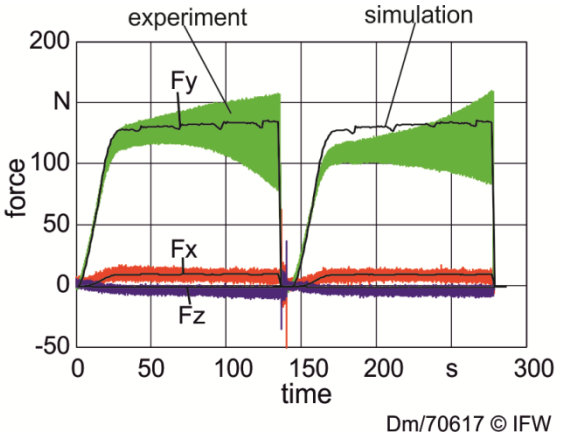

Fig. 7.21 Calculated (black lines) and measured grinding forces (oscillating lines) for the grinding of two flutes of a tungsten carbide tool. (Grinding wheel: Q-Flute-2 D54 C75, R = 62 mm, Workpiece: Tungsten Carbide, L = 100 mm, d = 10 mm, Process: Down Grinding, v_{ft} = 30 mm/min, v_c = 18m/s)

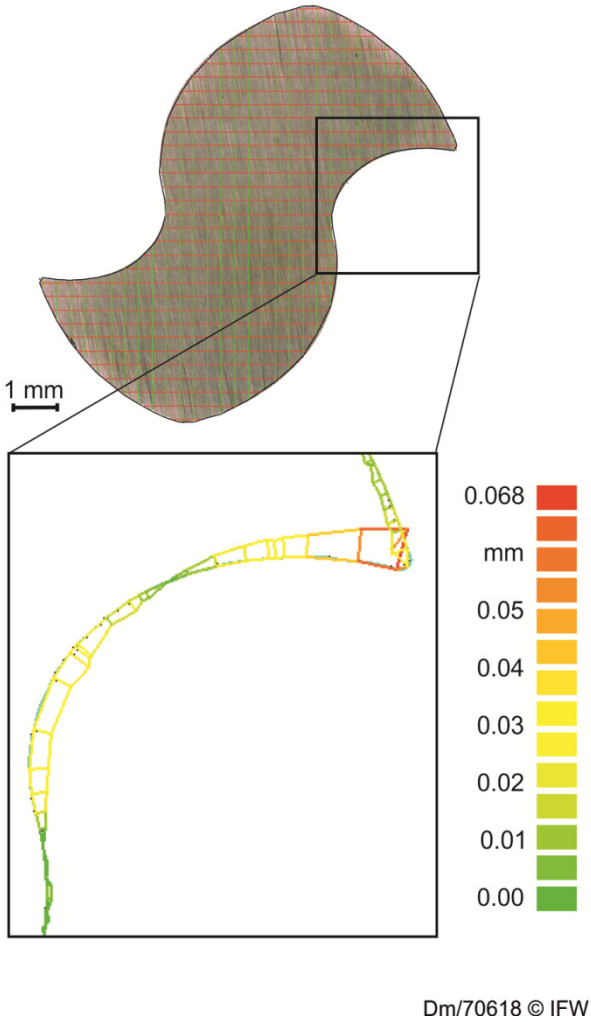

Fig. 7.22 Comparison of simulated cross-section using dexel-model and real cross-section (photograph made with digital microscope); detail shows part of the contour with highest deviation

workpiece, are predicted precisely by the simulation model, 3) The grinding forces slightly rise during full-contact phase, both in simulation and measurement. This effect is caused by the increasing stiffness of the workpiece when approaching the workpiece clamping and the resulting higher actual depth of cut at the end of each flute. 4) When grinding the second flute the simulated magnitude of F_y does not exactly match the measured values.

Apart from the grinding forces, the resulting cross-section of the workpiece has been simulated and compared with measurements. A Keyence optical microscope was used to create a high resolution picture of the cross-section of the workpiece tip, where the maximum shape error occurs. As can be seen in Figure 7.22, the difference between simulation and measurement is relatively low, which verifies the high accuracy of the developed and implemented static process machine interaction model. However, the cross-section resulting from grinding a flexible workpiece is different from the ideal cross-section, which can be simulated using a rigid workpiece, compare Figure 7.30.

7.6.2 Simulation of Dynamic Effects

The dynamic behavior of the workpiece and grinding wheel fixation as well as the grinding wheel topography have a wide influence on the process forces and the workpiece geometry. Due to the long computing time the dynamic effects are analyzed on geometrically simpler experiments, where a longitudinal flute is ground. The workpiece has a diameter of 10 mm and a cantilevering length of 100 mm. For the experiments and the simulation the adjusted depth of cut is 1 mm, the feed speed is 100 mm/min and the cutting speed is set to 18 m/s. A flute of 30 mm length is simulated with the introduced grinding process model; and the forces and workpiece geometry are calculated.

7.6.2.1 Influence of the Grinding Wheel Topography

The wavy wheel surface causes fluctuations in the process forces due to varying contact conditions. In Figure 7.23, calculated process forces with an ideal round grinding wheel and with a grinding wheel including an out-of-roundness of 24 µm, a harmonic wave of 10^{th} order with an amplitude of 1 µm and stochastically distributed grains of about 0.6 µm are shown. For the simulations, the dynamic module from Section 7.3.5.3 is included. Additionally, the measured force signals are also illustrated.

In the first few seconds, the contact length between grinding wheel and workpiece increases as well as the mean value and the amplitude of the process forces until the contact length gets quasi-constant. Comparing the mean values it is visible that the calculation with ideal round grinding wheel fits the measured data well for the *y*-direction, whereas for the *x*-direction the forces are overestimated. The calculation with the wavy grinding wheel shows a smoother change between running-in period and constant interval, similar to the measurements. For the *y*-direction the forces are underestimated by about 10 N, whereas in *x*-direction the simulation is in accordance with the measured data.

When comparing the amplitudes of calculated and measured forces, the high fluctuation at the beginning of the experiments is not expressed by the simulation. This is due to ideal initial conditions for the simulation. During the experiments,

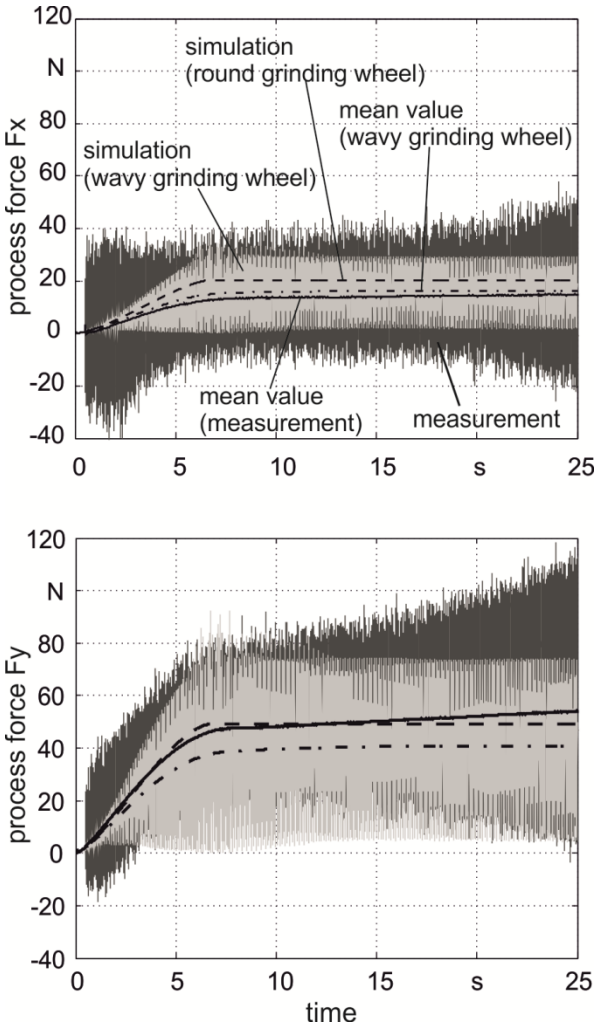

Fig. 7.23 Calculated process forces Fx and Fy with an ideal round and a wavy grinding wheel compared with measured data

influences of the coolant, for example, are also included in the measured force signal, which causes larger amplitudes at the beginning of the process. For the normal forces in *y*-direction, the increasing measured force amplitudes are also not represented by the simulation but quasi-constant amplitudes are reached. This characteristic can also be related to the coolant, which has a higher influence in normal direction than in tangential direction. The accuracy could be increased by means of additional analyses about the influence of coolant.

The consideration of the time histories of measured forces and the resulting time-varying coefficient of friction show significant periodic fluctuations, which depend on grinding wheel rotation, amplitude of the process parameters, feed, cutting speed and feed rate. Worth mentioning is the measured phase shift between the normal and tangential load, which is found in the measurements vary in severity and comparative measurements with other materials and fixations. As an example, the relationship between the local friction coefficient and the acting normal force F_N is displayed for different depths of cut in Figure 7.24.

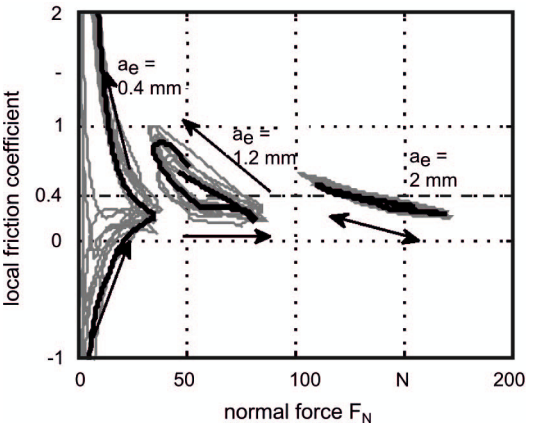

Fig. 7.24 Consideration of the timing behavior of the friction coefficient as a function of the normal force and the depth of cut

7.6.2.2 Influence of the Dynamic Effects on Workpiece Geometry

When comparing the results of the workpiece geometry by including the dynamic behavior of workpiece and grinding wheel, a difference in the geometry to the ideal surface is visible, as shown in Figure 7.25.

This difference has its maximum at the tip of the workpiece, when the forces cause the largest bending and decrease towards the clamping. When comparing the surface with single measured data points, the calculated geometry error is underestimated but shows qualitatively the same shape. The difference can be explained by the influence of the coolant, which is not represented in the simulation. By considering an additionally measured coolant-force component of about 10 N, as discussed in Section 7.6.2.1, the bending of the workpiece increases and the geometry error gives a better approximation of the measured data points.

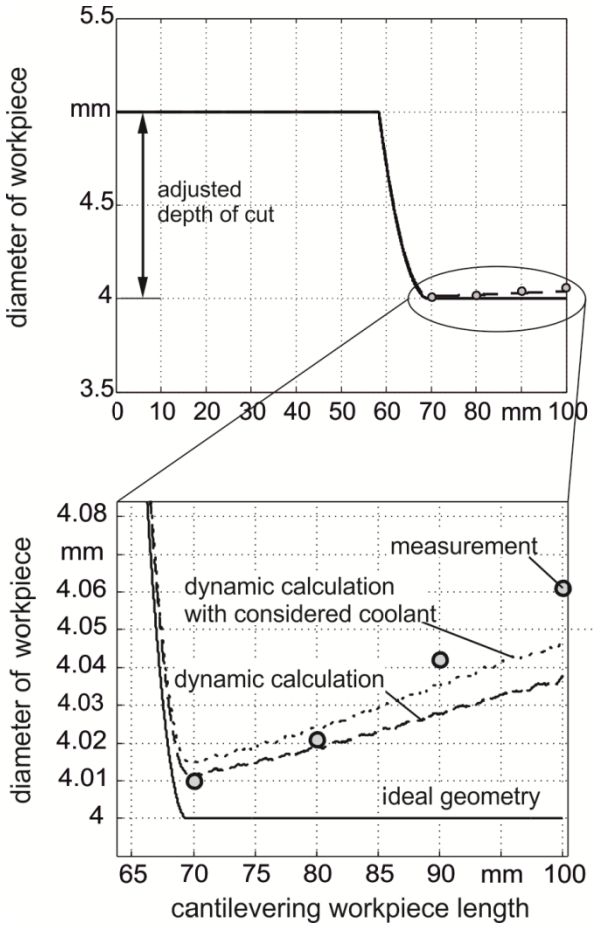

Fig. 7.25 Calculated workpiece geometry predicted by the dynamic module with and without coolant consideration

7.6.3 Simulation Studies

The presented computation models have been implemented as a plugin into the simulation system CutS, which has been developed at the IFW Hannover [8]. CutS is a universal framework for the simulation of machine movements and material removal and for the determination of technological process characteristics of manufacturing processes. It is possible to change the shapes and dimensions of workpiece and grinding wheel and to use different tool paths by loading NC-programs to the NC-control of CutS. Since the developed calculation models are not bound to one specific workpiece geometry or process parameter combination, it is possible to use CutS for simulation studies to gain more knowledge on tool grinding processes.

In order to determine suitable parameters such as dexel grid distance or simulation time step, simulation studies on the influence of these parameters on the simulation accuracy have been performed. Figure 7.26 shows the influence of the dexel grid distance on the resulting cross-section area of the workpiece, measured along the fluted part of the workpiece (mean value and min-max-bar). The higher the number of dexels used for simulation, the lower is the grid distance and the better is the simulation accuracy. It is noticeable that the mean value of the cross-section area is nearly the same for all grid distances but there is a variation for larger grid distances which can be up to 5 times the grid distance. The dexel grid distance should be chosen smaller than 0.1 mm for achieving high quality simulation results.

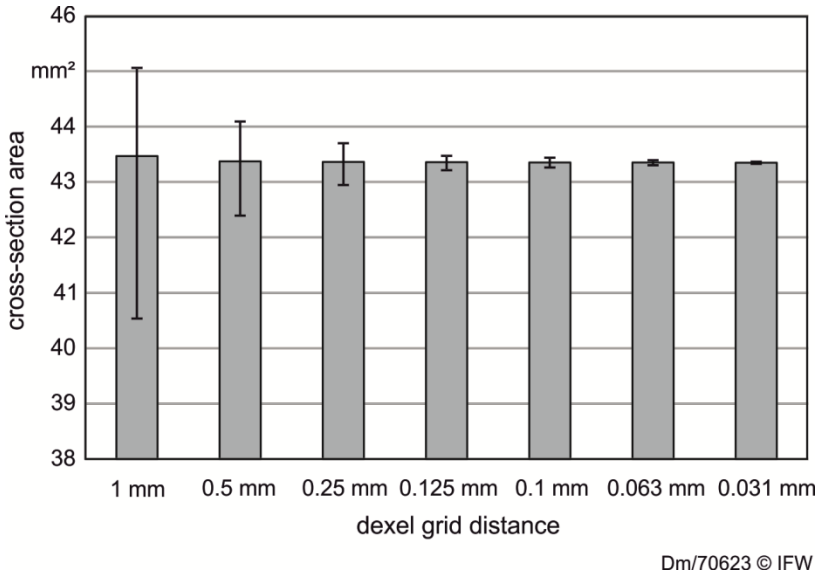

Fig. 7.26 Influence of dexel grid distance on simulation accuracy for calculating the workpiece cross section of a ground two-flute twist drill (10 mm diameter, 30 ° helix angle)

Another important simulation parameter is the simulation time step, which is the period of time represented by one simulation step. A lower simulation time step leads to better results and longer computation times. Figure 7.27 displays the influence of the time step on the simulation accuracy, described by the resulting cross section area. For large time steps, the simulation accuracy is very low, which is caused by the errors of the linear interpolation of the tool movement. For small time steps the interpolation error is negligible, because the difference between two tool positions is low and its movement can be linearized. Summarizing the results from Figure 7.27, a simulation time step of 0.5 seconds or lower should be applied, the lower the better.

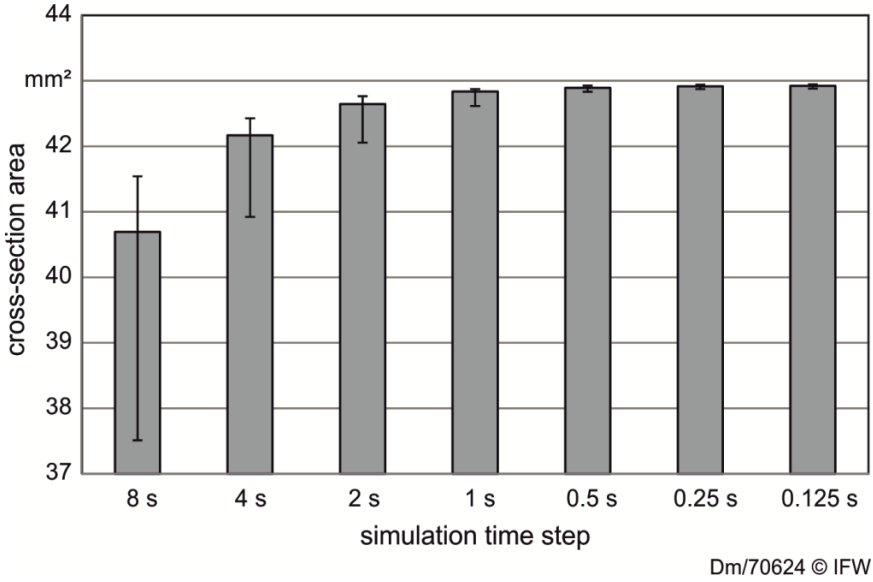

Fig. 7.27 Influence of simulation time step on simulation accuracy for calculating the workpiece cross section of a ground two-flute twist drill (dexel grid distance: 0.1 mm)

Another application of the simulation system is the analysis of technological relationships in tool grinding processes. Figure 7.28 exemplarily shows the influence of the feed velocity v_{fi} on the resulting process forces for grinding a two-flute tungsten carbide twist drill with 10 mm diameter. In the analyzed parameter limits, the process forces show a non-linear dependency on the feed velocity which reflects the relationship of the process force model as shown in Figure 7.15.

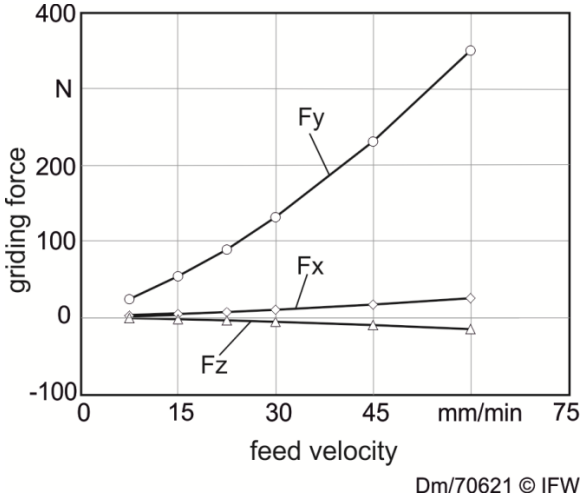

Fig. 7.28 Influence of feed velocity on calculated process forces accuracy for calculating the workpiece cross section of a ground two-flute twist drill (simulation time step: 0.5 s, dexel grid distance: 0.1 mm, for process parameters, see Figure 7.21)

7.6.4 Optimization

The main objective of the research on process machine interaction is to understand the occurring effects during grinding and to predict process characteristics and process outcome. With this knowledge, it is possible to optimize grinding processes already in the process planning phase. In this case, the developed models have been used to adapt the path of the grinding wheel to reduce the shape errors in the ground workpiece.

The optimization procedure starts with a simulation of the static workpiece deflection using the simulation model described in Section 7.6.1. During the simulation, the workpiece deflection is computed at the point, where the grinding wheel exits the contact area. At that point, the final flute profile is generated. Therefore, it is a good position to evaluate resulting shape error. A characteristic deformation profile for a two-flute tool is shown in Figure 7.29. It can be seen that the deflection constantly rises during the entrance phase of the grinding wheel and then decreases quadratically during full engagement due to the increasing stiffness of the workpiece near the clamping. The deflection v in y-direction of the second flute is significantly higher because of the reduced stiffness of the workpiece after grinding the first flute.

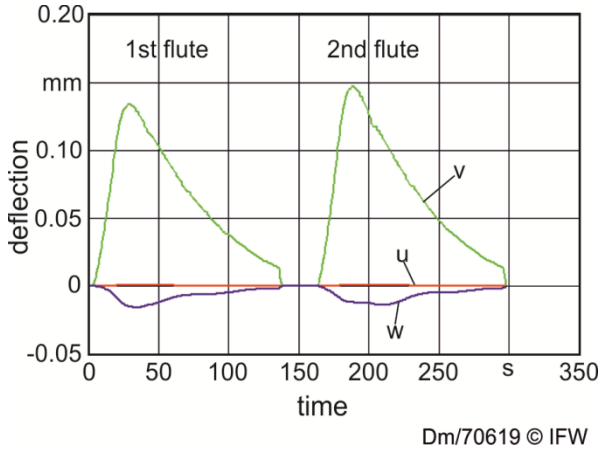

Fig. 7.29 Calculated workpiece deflection (u,v,w) in (x,y,z)-direction at current position of grinding wheel

The next step is the segmentation of the calculated workpiece deformation into line elements. These elements are then translated into NC commands, which change the movements of the grinding wheel. With the new NC-program, the simulation of the deformation is repeated until the desired shape of the workpiece is achieved. In this research, two optimization criteria are used to evaluate the current shape of the workpiece. The first criterion is the difference of the core radius of simulated and ideal cross-section. The second criterion is the dexel-wise comparison of the shape of a simulated ideal cross-section.

When the current NC-program leads to a workpiece shape fulfilling the quality criteria, the optimization procedure is stopped. As an exemplary result, Figure 7.30 compares the cross-sections at the tip of a workpiece for two different simulation runs with the ideal cross-section. The first cross section (left) has been simulated using the original NC-program. A relatively large deviation of the resulting workpiece shape from the ideal workpiece shape is visible with a maximum deviation of 160 µm, which corresponds to the deflection presented in Figure 7.29.

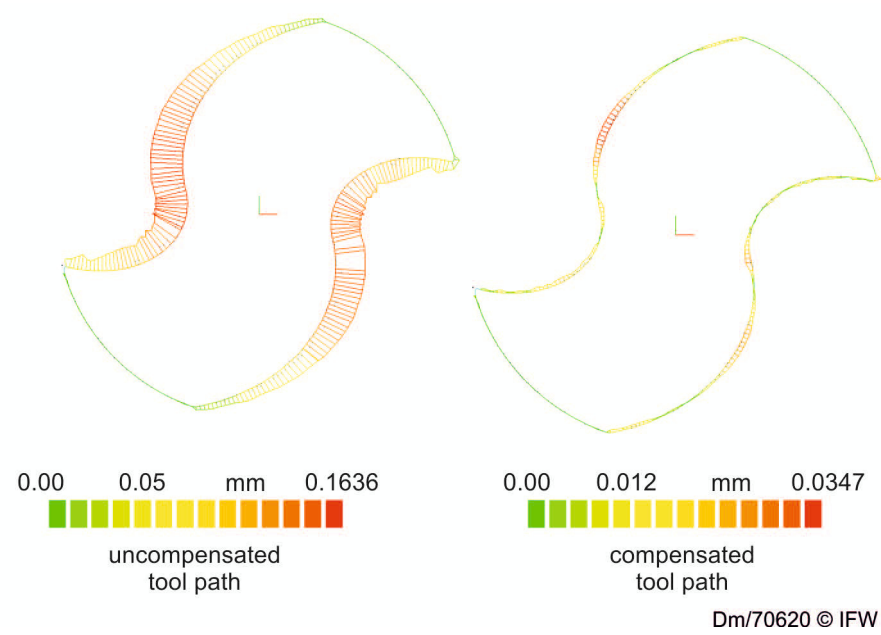

Fig. 7.30 Comparison of resulting workpiece cross-sections with uncompensated NC-program (left) and compensated tool path (right)

The cross-section on the right of Figure 7.30 has been computed using an adapted NC-program, which was the result of one optimization loop. It can be seen that the error has been reduced significantly with a maximum deviation of 35 µm. The results indicate that the presented optimization procedure is able to improve the workpiece quality in tool grinding, considering the existing process machine interactions.

7.7 Conclusion and Outlook

An interdisciplinary modeling approach to predict the process machine interaction in tool grinding has been presented. Models for the grinding process and the mechanical behavior of workpiece and machine have been developed and coupled with each other. A simulation of the process kinematics has been combined with a

dexel-based material removal simulation to compute the varying workpiece shape during the grinding of cutting tools. It has been possible to calculate the grinding forces and the static and dynamic deflections occurring during tool grinding. For the first time, it has been possible to calculate the stress distribution in the complex contact area. For this purpose, an empirical grinding force model was developed, which connects the acting stress with the equivalent depth of cut h_{eq} divided by the local contact length dl_g. A finite element approach to calculate the stress due to the microscopic grain engagement shows a high influence of the Young's modulus and the damage criteria. Based on the geometry-dependent mechanical properties of the workpiece and the simulated contact forces, the quasi-static and time-variant deflections can be predicted. The presented approaches have been validated by comparing measured and simulated workpiece geometry after grinding. In addition, the developed simulation methods have been used to optimize the path of the grinding wheel for a reduction of geometry errors of the ground tool. Since the modeling approach is designed modularly it can be extended continuously in the future, e. g. to include other grinding wheels or workpiece materials.

References

[1] European Cutting Tool Association: Zerspanungswerkzeuge: Marktvolumen weltweit, Fertigung Sonderausgabe – Werkzeuge 12, 7 (2010)

[2] Aurich, J.C., Biermann, D., Blum, H., Brecher, C., Carstensen, C., Denkena, B., Klocke, F., Kröger, M., Steinmann, P., Weinert, K.: Modelling and Simulation of Process - Machine Interaction in Grinding Production Engineering, vol. 3, pp. 111–120 (2008)

[3] de Payrebrune, K., Kröger, M., Deichmueller, M., Denkena, B.: Investigation on the Dynamics of Tool Grinding, Machine Dynamics Problems, vol. 33, pp. 92–104 (2009)

[4] Popp, K., Kröger, M., Deichmueller, M., Denkena, B.: Analysis of the Machine Structure and Dynamic Response of a Tool Grinding Machine. In: 1st International Conference on Process Machine Interactions, pp. 299–307 (2008)

[5] Popp, K., Kröger, M., Deichmueller, M., Denkena, B.: On Contact Modeling of Workpiece and Grinding Wheel with Nonlinear Elements. In: 7th EUROMECH Solid Mechanics Conference, pp. 281–282 (2009)

[6] Chang, H.-C., Wang, J.-J.J.: A stochastic Grinding Force Model considering Random Grit Distribution. International Journal of Machine Tools and Manufacture 48, 1335–1344 (2008)

[7] van Hook, T.: Real-Time Shaded NC Milling Display ACM SIGGRAPH Computer Graphics, vol. 20, pp. 15–20 (1986)

[8] Denkena, B., Böß, V.: Technological NC Simulation for Grinding and Cutting Processes Using CutS. In: 12th CIRP Conference on Modelling of Machining Operations, vol. II, pp. 563–566 (2009)

[9] Biermann, D., Mohn, T.: A Geometric-Kinematical Approach for the Simulation of Complex Grinding Processes. In: 6th CIRP International Conference on ICME (2008)

[10] Denkena, B., Tracht, K., Yu, J.-H.: Advanced NC-Simulation based on the Dexelmodel and the HRMC-Algorithm Production, Engineering, vol. XIII(1), pp. 91–94 (2006)

[11] de Payrebrune, K., Kröger, M.: Modal Reduction of Dynamics of Tool Grinding. In: 2nd International Conference on Process Machine Interactions (2010)
[12] Denkena, B., Deichmueller, M., Kröger, M., Popp, K.M., Carstensen, C., Schroeder, A., Wiedemann, S.: Geometrical Analysis of the Complex Contact Area for Modeling the local Distribution of Process Forces in Tool Grinding. In: 1st International Conference on Process Machine Interactions, pp. 289–298 (2008)
[13] Han, W., Reddy, D.: Plasticity. Springer (1999)
[14] Brokate, M., Carstensen, C., Valdman, J.: A Quasi-Static Boundary Value Problem in Multi-Surface Elastoplasticity. I: Analysis, Math. Methods Appl. Sci. 27(14), 1697–1710 (2004)
[15] Schröder, A., Wiedemann, S.: Error Estimates in Elastoplasticity using a Mixed Method, Humboldt Universität zu Berlin, Institute of Mathematics, Preprint 11-01 (2011)
[16] Schröder, A.: Mixed Finite Element Methods of Higher-Order for Model Contact Problems. Humboldt Universität zu Berlin, Institute of Mathematics, Preprint 09-16, submitted to SINUM (2009)
[17] Schröder, A., Wiedemann, S.: Humboldt Universität zu Berlin, Institute of Mathematics, Preprint 11-02 (2011)
[18] Schröder, A.: Constraints coefficients in *hp*-FEM. Numerical Mathematics and Advanced Applications, 183–190 (2008)
[19] Schröder, A.: Constrained approximation in *hp*-FEM: Unsymmetric subdivisions and multilevel hanging nodes. LNCSE, vol. 1(76), pp. 317–325 (2009)
[20] Han, W., Reddy, D.: On the Finite Element Method for Mixed Variational Inequalities arising in Elastoplastiity. SINUM 32(6), 1778–1807 (1995)
[21] Brokate, M., Carstensen, C., Valdman, J.: A quasi-static Boundary Value Problem in Multi-Surface Elastoplasticity. II: Numerical Solution, Math. Methods Appl. Sci. 28(8), 881–901 (2005)
[22] Wang, C.Y., Clausen, R.: Marble Cutting with Single Point Cutting Tool and Diamond Segments. Machine Tools & Manufacture 42, 1045–1054 (2002)
[23] Lemaitre, J., Desmorat, R.: Engineering Damage Mechanics. Springer (2005)
[24] Deichmueller, M., Denkena, B., de Payrebrune, K.M., Kröger, M., Wiedemann, S., Schroeder, A., Carstensen, C.: Determination of Static and Dynamic Deflections in Tool Grinding using a Dexel-Based Material Removal Simulation. In: 2nd CIRP International Conference on Process Machine Interactions (2010)
[25] Tönshoff, H., Peters, J., Inasaki, I., Paul, T.: Modelling and Simulation of Grinding Processes. CIRP Annals - Manufacturing Technology 41, 677–688 (1992)